2011

Theory of the scattering of light and surface plasmon polaritons by finite-size subwavelength metallic defects via field decomposition

Guangyuan Li

Feng Xiao
Edith Cowan University

Lin Cai

Kamal Alameh
Edith Cowan University

Anshi Xu

10.1088/1367-2630/13/7/073045
Li, G., Xiao, F. , Cai, L., Alameh, K. , & Xu, A. (2011). Theory of the scattering of light and surface plasmon polaritons by finite-size subwavelength metallic defects via field decomposition. New Journal of Physics, 13, 15p. Available here

Physical insight into the interactions among free space light, surface plasmon polaritons and quasi-cylindrical waves in subwavelength metallic gratings

Guangyuan Li[1]‡, Feng Xiao[2], Lin Cai[1], Kamal Alameh[2], and Anshi Xu[1]

[1]State Key Laboratory of Advanced Optical Communication Systems and Networks, School of Electronics Engineering and Computer Science, Peking University, Beijing, 100871, China

[2]WA Center of Excellence for MicroPhotonic System, Electron Science Research Institute, Edith Cowan University, Joondalup, WA, 6027, Australia

E-mail: gyli_2008@hotmail.com

Abstract. We provide a physical insight into the interactions among free space light, surface plasmon polaritons (SPPs), and quasi-cylindrical waves (CWs) in a subwavelength metallic grating composed of surface defects. The scattering properties of CWs are clarified, and the CW-related coefficients, which cannot be calculated by classical scattering theory, are shown to be obtained by decomposition of the generated fields when a surface defect is launched by the free-space light, a SPP or a CW. Results show that the SPP- and the CW-generation coefficients under the SPP incidence are approximate to their counterparts under the CW incidence for a single defect. Based on the concept of field decomposition and the elementary scattering processes of the free-space light, a SPP and a CW by a single defect, two SPP-CW models are developed to provide an intuitive picture of the interactions in the excitation and reflection of the SPP mode by N defects. The theoretical models are verified to be of high accuracy using exhaustive computation with various geometrical parameters over a broad spectral range from the visible to the thermal infrared regime.

PACS numbers: 73.20.Mf, 42.25.Fx, 78.67.-n

Submitted to: *New J. Phys.*

‡ Author to whom any correspondence should be addressed.

1. Introduction

Surface plasmon polaritons (SPPs) are electromagnetic surface modes confined to and propagating along the interface between a metal and a dielectric. To couple or decouple light to SPPs, an array of gratings on a metal film, known as the Kretschmann configuration, has been widely used. Gratings of various geometries such as nanoholes [1], air grooves [2], and metallic ridges [3] have been investigated theoretically or experimentally. A subwavelength slit supplemented with a periodic array of grooves (i.e., the slit-groove structure), or its three-dimensional equivalent, the so-called bull's eye structure has been attracting great attention in novel optical detectors [4, 5, 6]. Moreover, as metallic gratings are also capable to reflect SPPs, they have been used in various plasmonic devices including the unidirectional [7, 8] or bidirectional [9] coupler, and nano-cavities [10].

As the propagation length of the SPP mode along the air-metal (gold or silver) interface is tens of micrometers at the visible and near infrared regimes, the metallic gratings should be carefully designed to improve the efficiency of the specific usage. As a result, a quantitative knowledge of the SPP excitation and reflection efficiencies, which is a key issue in engineering related plasmonic devices, has aroused extensive concern. Until now most work has been done using numerical simulation techniques such as the finite element method [11], or theoretical methods such as the Green tensor approach [12, 13, 14], the Rayleigh expansion [15], the modal expansion technique [16, 17, 18], and the multiple-multipole method [19]. These methods, though accurate, suffer from large numerical cost especially when the number of defects is very large. What is worse, via these methods, the underlying physics is not clear enough.

To circumvent these problems, the involved interactions between the free-space light and the subwavelength metallic gratings should be clarified first. Though there were debates on the role of SPPs [20, 21, 22], it has been widely accepted that SPPs are the primary vector of the interactions at visible frequencies [22]. Accordingly, a microscopic theory has been proposed to provide physical insights into the extraordinary optical transmission (EOT) through subwavelength hole arrays [23]. With this theory, some of the authors have developed quantitative theoretical models for the EOT through a slit surrounded with symmetric [24] or asymmetric [25] periodic grooves, and for the SPP-Bragg reflectors composed of various defects [26]. These models provide clear pictures of the underlying physics and greatly simplify the structure design. As all these models incorporate only SPPs, they are referred to as pure SPP models. The residual field referred to as the quasi-cylindrical wave (CW), which was proposed theoretically in [22] and then demonstrated experimentally in [27], has not been considered, resulting in pronounced deviations between model predictions and fully vectorial computational data.

Recently, the cross conversion between SPPs and CWs, specifically the CW-to-SPP conversion was proposed in [28]. With consideration of this conversion, the SPP excitation efficiency by a metallic groove doublet under normal illumination of the free-

space light was accurately predicted. This work was then theoretically reexamined by the authors [29]. The SPP-to-CW conversion as well as the reflection and transmission of the CW was further proposed. With these elementary scattering processes incorporated, a SPP-CW model was proposed accordingly to predict the SPP excitation efficiency by N periodic grooves with accuracy. Quite recently, a hybrid-wave model was also proposed and shown to be accurate to predict the field at the air-metal interface [30] and the EOT through the hole array [31]. However, the underlying cross conversion processes between SPPs and CWs are not clear in the model. Moreover, as CWs are not normal modes (they are a superposition of modes), there are no scattering matrices for them according to the classical theories [32], and one may think that it is difficult (or even impossible) to define scattering coefficients for those waves [30, 33]. As a result, it is necessary to clarify the the scattering of CWs and especially the related coefficients used in our previous work [29].

In this work, we will provide a physical insight into the interactions among the free space light, SPPs and CWs in subwavelength metallic gratings. In Section 2, we summarize the elementary scattering processes of the light, the SPP and the CW by the simplest structure, i.e., a single surface defect. The scattering of CWs and the method to calculate the CW-related coefficients by field decomposition are clarified. The interactions in a metallic grating composed of finite number of defects, periodic or aperiodic, are discussed in Section 3. Accordingly, two SPP-CW models for the SPP excitation and reflection efficiencies will be developed to provide an intuitive picture. The models' validity will be quantitatively tested using exhaustive calculations with various parameters. For the sake of readability, we only use the rectangle air groove as the defect to illustrate our discussions. The models and conclusions are also applicable to other types of defects such as the metallic or dielectric ridges, as the surface defect is treated as a "black box", just as done in our previous work [26]. Gold is used with the frequency-dependent permittivities tabulated in [34]. Without special specification, the analysis will be provided for $\lambda = 800\,\mathrm{nm}$.

2. A single subwavelength groove

We first focus on the simplest case, the scattering of the plane wave, the SPP mode and the CW by a single groove, as shown in figure 1. As we restrict ourselves to the magnetic field (i.e., H_y) at the dielectric-metal interface ($z = 0$), the out-going radiations generated by the SPP incidence or the CW incidence, as shown in figures 1(b) and 1(c), respectively, will not be considered in this paper.

To understand the scattering processes and the related coefficients, we first briefly introduce the concepts of the zero field and the scattered field. In a scattering problem, the zero field is the field when there are no scatters at all; the scattered field is calculated by subtracting the zero field from the total field that with scatters. For example, when a plane wave is incident on a single groove, as shown in figure 1(a), the zero field is the field when there is no groove, i.e., the field in the multi-layer geometry only composed

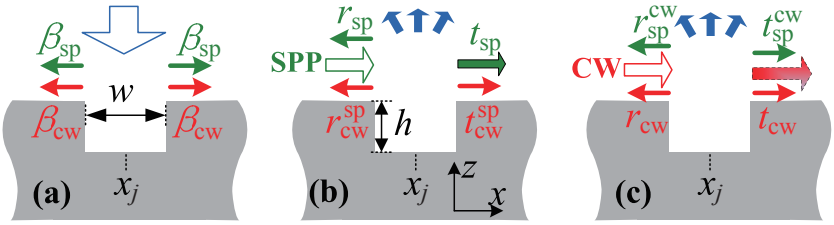

Figure 1. The decomposition of the magnetic fields at the surface into SPPs (green) and CWs (red) is performed for the scattering of (a) a normally incident free-space light polarized along the x axis (TM-polarized), (b) a SPP, and (c) a CW by a single groove of width w, depth h, and center in the x-direction x_j. The coefficients $\beta_{\rm cw}, \beta_{\rm sp}, r_{\rm sp}, t_{\rm sp}, r_{\rm cw}^{\rm sp}, t_{\rm cw}^{\rm sp}, r_{\rm sp}^{\rm cw}, t_{\rm sp}^{\rm cw}, r_{\rm cw}, t_{\rm cw}$ are all defined in the text.

of the dielectric layer and the metal layer. In this case, the zero field can be calculated analytically.

2.1. The field decomposition into SPPs and CWs

As stated in [33], both SPPs and CWs are generated under the light illumination or a slit mode incidence. When a single groove with the center in the x-direction being x_j is illuminated by a normally incident TM-polarized plane wave, as shown in figure 1(a), the scattered magnetic field $H_y^{\rm sc}(x)$ launched at the interface on every side of the groove can be accurately described as a combination of a SPP and a CW [28],

$$H_y^{\rm sc}(|x-x_j|>w/2) = \beta_{\rm sp}\exp({\rm i}k_0 n_{\rm sp}|x-x_j|) + \beta_{\rm cw} v(|x-x_j|), \tag{1}$$

where $k_0 = 2\pi/\lambda$, $n_{\rm sp} = n_{\rm d}n_{\rm m}/\sqrt{n_{\rm d}^2+n_{\rm m}^2}$ is the effective refractive index of the SPP mode along the dielectric-metal interface with $n_{\rm d}$ being the refractive index of the dielectric and $n_{\rm m}$ being that of the metal, $\beta_{\rm sp}$ is the SPP excitation coefficient and $\beta_{\rm cw}$ is the CW excitation coefficient, $v(x) \approx W(2\pi\gamma|x|/\lambda)/W(2\pi\gamma)(\lambda/|x|)^{3/2}\exp({\rm i}k_0 n_{\rm d}x)$ with $W(t) = -2\sqrt{-{\rm i}t/\pi}\int_{-\infty}^{\infty} z^2\exp(-z^2)/(z-\sqrt{-{\rm i}t}){\rm d}z$ and $\gamma = n_{\rm sp}-n_{\rm d}$ [33]. Note that here we use the scattered fields instead of the total fields since SPPs do not occur in the zero fields, but show up in the scattered fields at the surface of the metal [35]. $\beta_{\rm sp}$ can be calculated analytically [36] or numerically by using the method incorporating the mode orthogonality as mentioned in [33]. $\beta_{\rm cw}$ is then obtained by setting $|x-x_j|=\lambda$ in (1) as $v(\lambda)=1$. Figure 2 shows that the excitation coefficients calculated through the field decomposition in the form of (1) are very accurate. Note that the dielectric is assumed to be air with $n_{\rm d}=1.0$ throughout the paper.

We should emphasize that though the excitation coefficient of the CW cannot be calculated in a similar way to that of the SPP by using the mode orthogonality as the CW is not a normal mode, it can be obtained by the field decomposition. In other words, because the CW is defined as the residual field extracted by subtracting the SPP from the total scattered field, its excitation coefficient $\beta_{\rm cw}$ is then defined as the complex amplitude of the residual field whose propagation characteristics is in form of

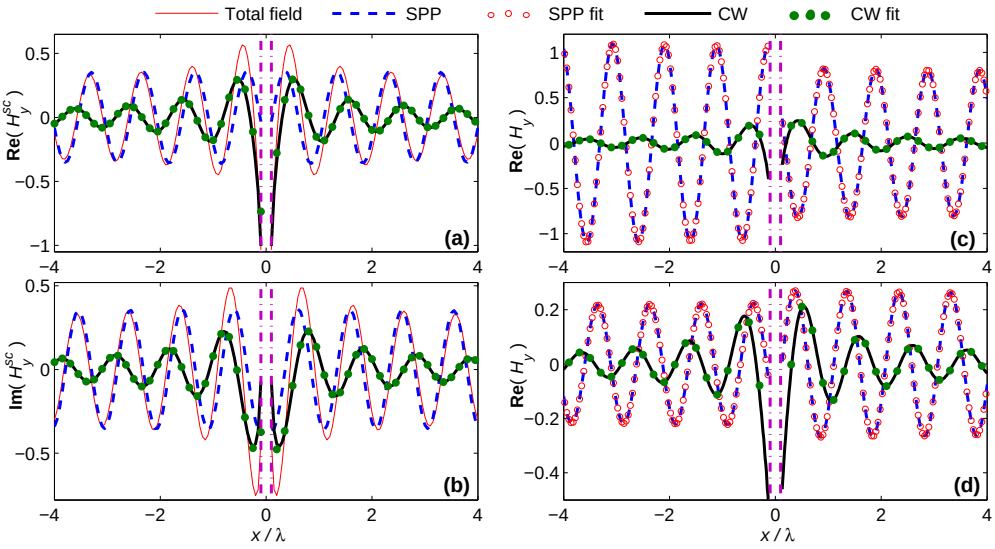

Figure 2. The total scattered magnetic fields at the interface ("Total field" in red-solid lines) are decomposed into SPPs and CWs. SPPs (blue-dashed lines) are obtained using (1) with $\beta_{\rm sp}$ calculated numerically, CWs (black-solid lines) are then extracted by subtracting SPPs from the total scattered fields. Green dots show the CWs fitted using (1) with $\beta_{\rm cw}$ obtained by setting $|x - x_j| = \lambda$. In the figure, "Re" means the real part, and "Im" means the imaginary part. The calculations are performed with $w = 0.2\lambda$, $h = 0.2\lambda$, $x_j = 0$.

$v(x)$ and normalized as $v(|x| = \lambda) = 1$. This definition is quite different from $\beta_{\rm sp}$, which is defined according to the scattering theory and reciprocity [32]. This difference is very important to understand the scattering of SPPs and CWs that will be discussed later. We should emphasize that both $\beta_{\rm sp}$ and $\beta_{\rm cw}$ in (1) are calculated under the condition that the Poynting vector (or the power) of the incident plane wave is unity.

Now let us consider the scattering of a SPP mode by a single groove, as shown in figure 1(b). In this case, the zero field is exactly the incident SPP mode along the dielectric-metal interface. The generated forward-going and backward-going fields (i.e., the scattered fields) can also be decomposed into SPPs and CWs, similar to the scattering of the plane wave. If the incident SPP mode at the interface is expressed as $H^{\rm in}_{y,{\rm SPPin}} = H_0 \exp[{\rm i}k_0 n_{\rm sp}(x - x_j)]$ with H_0 being its complex amplitude at $x = x_j$, the reflected field (i.e., the generated backward-going field) and the transmitted field (i.e., the total forward-going field that is the sum of the zero field and the generated forward-going field) at the interface on every side of the groove are expressed as

$$H^{\rm ref}_{y,{\rm SPPin}}(x < x_j - w/2) = r_{\rm sp} H_0 \exp[-{\rm i}k_0 n_{\rm sp}(x - x_j)] + r^{\rm sp}_{\rm cw} H_0 v(x_j - x), \qquad (2a)$$

$$H^{\rm trans}_{y,{\rm SPPin}}(x > x_j + w/2) = t_{\rm sp} H_0 \exp[{\rm i}k_0 n_{\rm sp}(x - x_j)] + t^{\rm sp}_{\rm cw} H_0 v(x - x_j), \qquad (2b)$$

respectively, where $r_{\rm sp}$ and $t_{\rm sp}$ are the SPP reflection and transmission coefficients, $r^{\rm sp}_{\rm cw}$ and $t^{\rm sp}_{\rm cw}$ are defined as cross conversion coefficients associated to the scattering of the incident SPP into the generated backward- and forward-going CWs. As the SPP is a normal mode, its reflection and transmission coefficients are easy to calculate according

to the mode orthogonality, similar to the corresponding process for calculating $\beta_{\rm sp}$. $r_{\rm cw}^{\rm sp}$ and $t_{\rm cw}^{\rm sp}$ are then calculated by setting $|x-x_j|=\lambda$ in (2). Note that as the transmitted SPP is the total field, the generated forward-going SPP mode (i.e., the scattered field) is expressed as $(t_{\rm sp}-1)H_0\exp[{\rm i}k_0n_{\rm sp}(x-x_j)]$. In other words, the corresponding forward-going SPP-generation coefficient is $t_{\rm sp}-1$.

For the scattering of a CW by a single groove, as shown in figure 1(c), the zero field is exactly the incident CW originated from x_i and expressed as $H_{y,\rm CWin}^{\rm in}(x)=H_1v(x-x_i)$ at the interface with $x_i<x_j-w/2$. The generated forward-going and backward-going fields (i.e., the scattered fields) at the interface on every side of the groove can also be decomposed into SPPs and CWs,

$$H_{y,\rm CWin}^{\rm ref}(x<x_j-w/2)=r_{\rm sp}^{\rm cw}H_2\exp[-{\rm i}k_0n_{\rm sp}(x-x_j)]+r_{\rm cw}H_2v(x_j-x), \qquad (3a)$$

$$H_{y,\rm CWin}^{\rm sc,trans}(x>x_j+w/2)=t_{\rm sp}^{\rm cw}H_2\exp[{\rm i}k_0n_{\rm sp}(x-x_j)]+t_{\rm cw}H_2v(x-x_j), \qquad (3b)$$

where $H_2=H_{y,\rm CWin}^{\rm in}(x=x_j)$, $r_{\rm sp}^{\rm cw}$ and $t_{\rm sp}^{\rm cw}$ are cross conversion coefficients associated to the scattering of the incident CW into the backward- and forward-going SPPs, $r_{\rm cw}$ and $t_{\rm cw}$ are the backward- and forward-going CW-generation coefficients, respectively. Note that the definitions of $r_{\rm sp}^{\rm cw}$ and $t_{\rm sp}^{\rm cw}$ are exactly the same as those of $r_{\rm c}$ and $t_{\rm c}$ in [28]. The calculation of the involved coefficients is the same as that of the scattering coefficients for the SPP incidence. We should emphasize that $r_{\rm sp}^{\rm cw}$, $t_{\rm sp}^{\rm cw}$, $r_{\rm cw}$ and $t_{\rm cw}$ are independent from x_i. Note that $t_{\rm cw}$ is quite different from the SPP transmission coefficient $t_{\rm sp}$. This difference is due to the fact that the transmitted SPP can be easily expressed in one term which includes the contributions from both the incident and the generated forward-going SPPs, whereas the transmitted CW should be expressed as the sum of the incident and the generated forward-going CWs,

$$\begin{aligned} H_{y,\rm CWin}^{\rm trans}(x>x_j+w/2) &= H_{y,\rm CWin}^{\rm in}(x)+H_{y,\rm CWin}^{\rm sc,trans}(x) \\ &= H_1v(x-x_i)+t_{\rm cw}H_2v(x-x_j). \end{aligned} \qquad (4)$$

Equation (4) cannot be incorporated in one term because of the complex propagation property of the CW.

The calculation of $r_{\rm sp}$, $t_{\rm sp}$, $r_{\rm sp}^{\rm cw}$ and $t_{\rm sp}^{\rm cw}$ is very convenient using the fully vectorial aperiodic Fourier modal method (a-FMM) [37], as the Fourier space-harmonic order of the SPP mode is easy to determine. $r_{\rm cw}^{\rm sp}$, $t_{\rm cw}^{\rm sp}$, $r_{\rm cw}$ and $t_{\rm cw}$ are then obtained by setting $|x-x_j|=\lambda$ in (2) and (3). Figure **??** shows the field decomposition and fitting. In the figure, the lines are the field components extracted directly from the a-FMM computational data, and the symbols are those fitted using (2) and (3) with the obtained coefficients. It is clear that the decomposition of the generated fields into SPPs and CWs for both the SPP incidence and the CW incidence are correct and all the related coefficients calculated by field decomposition are very accurate.

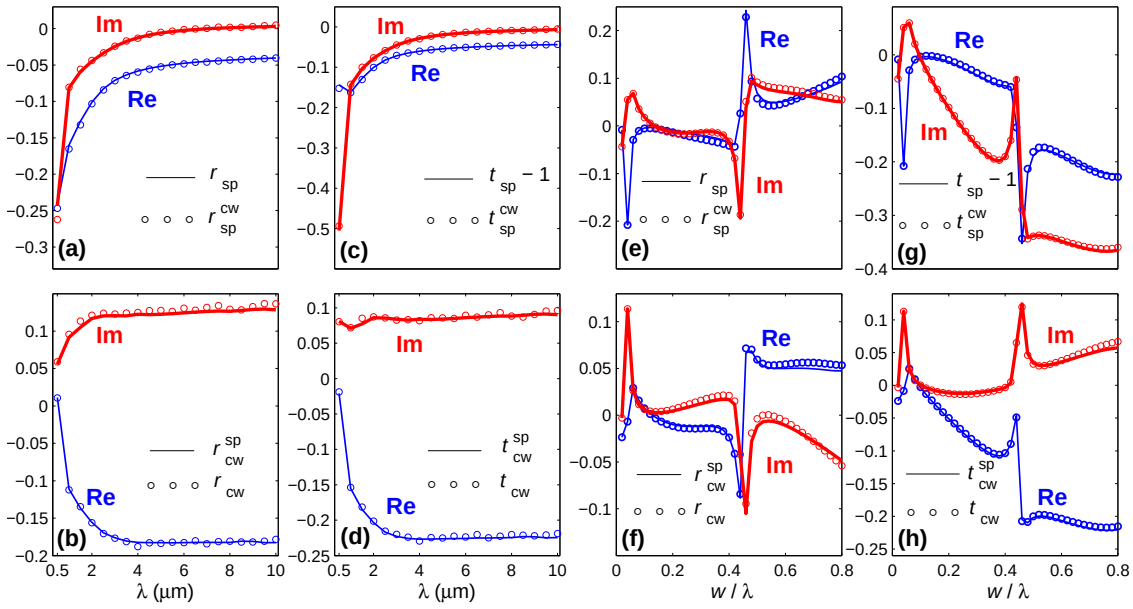

Figure 3. The behaviors of the four coefficient pairs (r_{sp}, r_{sp}^{cw}), $(t_{sp}-1, t_{sp}^{cw})$, (r_{cw}^{sp}, r_{cw}), and (t_{cw}^{sp}, t_{cw}) as functions of the operating wavelength with $w = 0.2\lambda$, $h = 0.2\lambda$, and of the groove width with $h = 0.4\lambda$, $\lambda = 0.8\mu$m. Blue lines and symbols are for the real parts, and red ones for the imaginary parts.

2.2. Relationship among the scattering coefficients

We notice that there is a remarkable relationship for the scattering coefficients of SPPs and CWs,

$$r_{\rm sp}^{\rm cw} \approx r_{\rm sp}, \qquad t_{\rm sp}^{\rm cw} \approx t_{\rm sp} - 1, \tag{5a}$$

$$r_{\rm cw} \approx r_{\rm cw}^{\rm sp}, \qquad t_{\rm cw} \approx t_{\rm cw}^{\rm sp}, \tag{5b}$$

where $(5a)$ is exactly the same as (5) in [28]. Equation (5) has been thoroughly validated for various geometries over a broad spectral range from the visible to the thermal infrared regime, as illustrated in figures 3. We have also performed exhaustive validations for various groove depths ranging from 0.02λ to 0.85λ, and also for the metallic or dielectric ridge of various widths and heights (not shown here due to the space limitations).

This approximation can be explained by the causality principle, just as done in [28]. The forward- and backward-going SPP-generation (or CW-generation) coefficients for the CW incidence should be the equal to their counterparts for the SPP incidence. In other words, the generated SPPs and CWs (i.e., the scattered fields) are identical for the incidence of a SPP and the incidence of a CW as the two incidences share many properties [28]. Note that here we use the generation coefficients instead of the transmission coefficients so that the zero fields are excluded for both the SPP incidence and the CW incidence. With these in mind, it is natural to understand the term $t_{\rm sp}-1$ instead of $t_{\rm sp}$ in $(5a)$. We should emphasize that $r_{\rm sp}^{\rm cw}$ (or $t_{\rm sp}^{\rm cw}$) may be not equal to $r_{\rm cw}^{\rm sp}$ (or $t_{\rm cw}^{\rm sp}$). This does not violate the reciprocity since CWs, which are not normal modes, do not obey the reciprocity according to the classic scattering theory [32].

This approximation is very useful since it considerably eases the calculation of the scattering coefficients. We need to calculate four coefficients instead of eight ones for the elementary scattering processes of the SPP and the CW by a single groove. As the incidence of a CW is a bit more complex than that of a SPP in the a-FMM, we suggest to calculate the four scattering coefficients of the SPP mode, i.e., $r_{\rm sp}, t_{\rm sp}, r_{\rm cw}^{\rm sp}$ and $t_{\rm cw}^{\rm sp}$.

3. N subwavelength grooves

In this section, we study the interactions in metallic gratings composed of N subwavelength grooves, specially the physics underlying the excitation and the reflection of the SPP mode, as shown in figure 4, which are important in plasmonic devices especially the slit-groove structure studied in our previous work [24, 25]. We should emphasize that the grooves may be periodic or aperiodic. Two intuitive SPP-CW models incorporating the whole elementary scattering processes shown by figure 1 will be developed, from which two pure SPP models are extracted by ignoring the existence of CWs. Exhaustive comparisons among the SPP-CW model predictions, the pure SPP model predictions, and the fully vectorial a-FMM computational data will be performed to validate the quantitative accuracy of the SPP-CW models, emphasizing that the SPP-CW models are reasonable and versatile to depict the interactions among the plane wave, SPPs and CWs in metallic gratings.

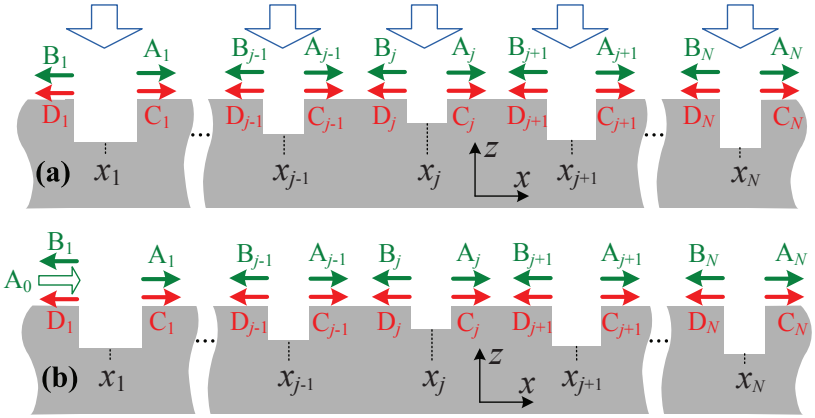

Figure 4. Schematics of the SPP-CW coupled-mode models for (a) the SPP excitation under the normal illumination of a TM-polarized plane wave, and (b) the SPP reflection by N grooves with width w_j, depth h_j, and their centers in the x axis being x_j, $j = 1, \cdots, N$. The electromagnetic quantities $A_0, \cdots, A_N$, $B_1, \cdots, B_N$, $C_1, \cdots, C_N$, $D_1, \cdots, D_N$ are all defined in the text.

3.1. The SPP-CW models

Let us consider the excitation of SPPs by N grooves under the normal illumination of a TM-polarized free-space light of unity Poynting vector, as shown in figure 4(a). The free-space light will generate left- and right-going SPPs and CWs at every groove.

The generated SPPs and CWs will then be further scattered by other grooves. Taking into account of all the elementary scattering processes of the plane wave, the SPP and the CW, as shown in figure 1, we develop a SPP-CW model for the SPP excitation coefficient by N grooves. In the SPP-CW model, A_j and B_j are the respective complex amplitudes of the right- and left-going SPPs propagating away from the groove "j", while C_j and D_j are those of CWs generated by the groove "j" ($j = 1, 2, \cdots, N$). Note that the definitions of A_j (or B_j) and C_j (or D_j) are quite different. This difference is due to the fact that the transmitted SPP incorporates the incident one, while the transmitted CW should be expressed by the sum of the incident CW and the generated forward-going CW, as has been clarified in (4). Bear these in mind, all the elementary scattering processes of the plane wave, SPPs and CWs are embodied in the following coupled-mode equations,

$$A_j = \beta_{sp,j} + t_{\mathrm{sp},j} u_{j-1} A_{j-1} + r_{\mathrm{sp},j} u_j B_{j+1} + t^{\mathrm{cw}}_{\mathrm{sp},j} \sum_{m=1}^{j-1} C_m V_{j,m} + r^{\mathrm{cw}}_{\mathrm{sp},j} \sum_{m=j+1}^{N} D_m V_{m,j}, \quad (6a)$$

$$B_j = \beta_{sp,j} + r_{\mathrm{sp},j} u_{j-1} A_{j-1} + t_{\mathrm{sp},j} u_j B_{j+1} + r^{\mathrm{cw}}_{\mathrm{sp},j} \sum_{m=1}^{j-1} C_m V_{j,m} + t^{\mathrm{cw}}_{\mathrm{sp},j} \sum_{m=j+1}^{N} D_m V_{m,j}, \quad (6b)$$

$$C_j = \beta_{cw,j} + t^{\mathrm{sp}}_{\mathrm{cw},j} u_{j-1} A_{j-1} + r^{\mathrm{sp}}_{\mathrm{cw},j} u_j B_{j+1} + t_{\mathrm{cw},j} \sum_{m=1}^{j-1} C_m V_{j,m} + r_{\mathrm{cw},j} \sum_{m=j+1}^{N} D_m V_{m,j}, \quad (6c)$$

$$D_j = \beta_{cw,j} + r^{\mathrm{sp}}_{\mathrm{cw},j} u_{j-1} A_{j-1} + t^{\mathrm{sp}}_{\mathrm{cw},j} u_j B_{j+1} + r_{\mathrm{cw},j} \sum_{m=1}^{j-1} C_m V_{j,m} + t_{\mathrm{cw},j} \sum_{m=j+1}^{N} D_m V_{m,j}, \quad (6d)$$

where $j = 1, \cdots, N$, $u_j = \exp[\mathrm{i}k_0 n_{\mathrm{sp}}(x_{j+1} - x_j)]$ with $u_0 = u_N = 0$, $V_{j,m} = v(x_j - x_m)$, $V_{m,j} = v(x_m - x_j)$, $A_0 = C_0 = B_{N+1} = D_{N+1} = 0$.

The right side of ($6a$) is interpreted as follows. The first term is corresponding to the SPP excitation coefficient of the groove "j" under the normal illumination of the plane wave. The second and the third terms mean the transmission and the reflection of SPPs propagating away from neighboring grooves on the left and right sides, respectively. The forth (the fifth) term is associated to the CW-to-SPP conversion for all the forward-going (backward-going) CWs generated by all the other grooves on the left (right) side. Other equations can be understood similarly. Note that A_j, B_j and C_j, D_j in (6) are treated differently because of their different definitions as have been emphasized.

The solving of the derived $4N$ linear equations is a routine and of negligible numerical cost for a practical N (usually smaller than 30). Once A_j, B_j, C_j, D_j ($j = 1, \cdots, N$) are obtained, the SPP excitation coefficient is then expressed as $\beta_N = A_N$ (the SPP excitation efficiency is $|\beta_N|^2$). The scattered magnetic fields at the surface in the region $x_{j-1} + w_{j-1}/2 < x < x_j - w_j/2$ are then expressed as

$$\begin{aligned} H_y^{\mathrm{sc}}(x, z = 0) \quad &= A_{j-1} \exp[ik_{sp}(x - x_{j-1})] + B_j \exp[-ik_{sp}(x - x_j)] \\ &+ \sum_{m=1}^{j-1} C_m v(x - x_m) + \sum_{m=j}^{N} D_m v(x_m - x) \end{aligned} \quad (7)$$

where we further set $x_0 + w_0/2 = -\infty$ and $x_{N+1} + w_{N+1}/2 = \infty$, so that Eq. (7) is always valid for $1 \le j \le N + 1$.

For the SPP reflection coefficient by N grooves, as shown in figure 4(b), the incident SPP mode is assumed to be of unity amplitude at $x = x_1$, i.e., $A_0 = 1$. The SPP-CW model for the SPP reflection and transmission coefficients are developed similarly to the model for the SPP excitation coefficient, with A_j, B_j, C_j and D_j ($j = 1, 2, \cdots, N$) of the same meanings as their counterparts in figure 4(a). It is obtained by simply deleting $\beta_{sp,j}, \beta_{cw,j}$ and setting $u_0 = A_0 = 1$ in (6). The SPP reflection and transmission coefficients are expressed as $r_N = B_1$, $t_N = A_N$ for (7) (the reflectance and transmittance are $R_N = |r_N|^2$ and $T_N = |t_N|^2$, respectively).

Note that in the SPP-CW models, the influences of the groove "j" are embodied by a set of coefficients, i.e., $\beta_{\mathrm{sp},j}, \beta_{\mathrm{cw},j}$, $r_{\mathrm{sp},j}, t_{\mathrm{sp},j}$, $r^{\mathrm{sp}}_{\mathrm{cw},j}, t^{\mathrm{sp}}_{\mathrm{cw},j}$, $r^{\mathrm{cw}}_{\mathrm{sp},j}, t^{\mathrm{cw}}_{\mathrm{sp},j}$, and $r_{\mathrm{cw},j}, t_{\mathrm{cw},j}$. In other words, each groove is treated as a "black box". As a result, the two SPP-CW models are also applicable for other types of surface defects such as the metallic or dielectric ridges. The approximation for the eight scattering coefficients of SPPs and CWs, i.e., (5) is used to reduce the complexity of the two models.

As a result, with the help of the SPP-CW models in forms of $4N$ linear equations, the excitation, the reflection and the transmission of the SPP mode by N grooves are described by the involved elementary scattering processes in a single groove. In such a way, the computational cost of β_N, r_N and t_N for N periodic defects is reduced into that of β_1, r_1 and t_1 for a single one.

3.2. The pure SPP models

When CWs are neglected, the SPP-CW models are reduced into the corresponding pure SPP models in forms of $2N$ linear equations simply by setting $C_j = D_j = 0$. Specially, if the N grooves are periodic with period p ($p = x_{j+1} - x_j$ and $u = u_j = \exp(\mathrm{i}k_0 n_{\mathrm{sp}} p)$ for $j = 1, \cdots, N-1$), width $w = w_j$ and height $h = h_j$ (for $j = 1, \cdots, N$), the pure SPP models can also be expressed in recursive forms,

$$\begin{aligned}
\beta_N &= \beta_{N-1} + \tau_{N-1} u \frac{\beta_1 + \beta_{N-1}\rho_1 u}{1 - \rho_{N-1}\rho_1 u^2}, \\
\rho_N &= \rho_1 + \rho_{N-1} \frac{\tau_1^2 u^2}{1 - \rho_{N-1}\rho_1 u^2}, \\
\tau_N &= \frac{\tau_{N-1}\tau_1 u}{1 - \rho_{N-1}\rho_1 u^2},
\end{aligned} \tag{8}$$

where $\beta_1 = \beta_{\mathrm{sp},1}$, $\rho_1 = r_{\mathrm{sp},1}$ and $\tau_1 = t_{\mathrm{sp},1}$ are the SPP excitation, reflection and transmission coefficients by a single groove, respectively, β_N, ρ_N, τ_N are those by N periodic grooves. For the deducing of (8), one can refer to our previous work on the SPP-Bragg reflector [26], where the equivalence between the linear equation forms and the recursive forms has also been demonstrated.

Note that we use $u = \exp(\mathrm{i}k_0 n_{\mathrm{sp}} p)$ here instead of $\exp[\mathrm{i}k_0 n_{\mathrm{sp}}(p - w)]$ in [26]. This is because the definitions of r_{sp} and t_{sp} used here are different from those used in [26]. In other words, the factor $\exp(-\mathrm{i}k_0 n_{\mathrm{sp}} w)$ has been incorporated in r_{sp} and t_{sp} used here.

3.3. Model validations

To validate the quantitative accuracy of the SPP-CW models and the pure SPP models, exhaustive comparisons will be performed by varying the period, the groove width and depth, the period number and the operating wavelength. For the sake of readability, we use periodic grooves and randomly select some geometrical parameters to illustrate our discussions. We should emphasize that this work is not intended to employ the optimized geometrical parameters, but to quantitatively validate the theoretical models incorporating the interactions in the metallic grating, which will pave the way for the structure design and optimization with clear physical insight as well as a great reduce of the computational cost.

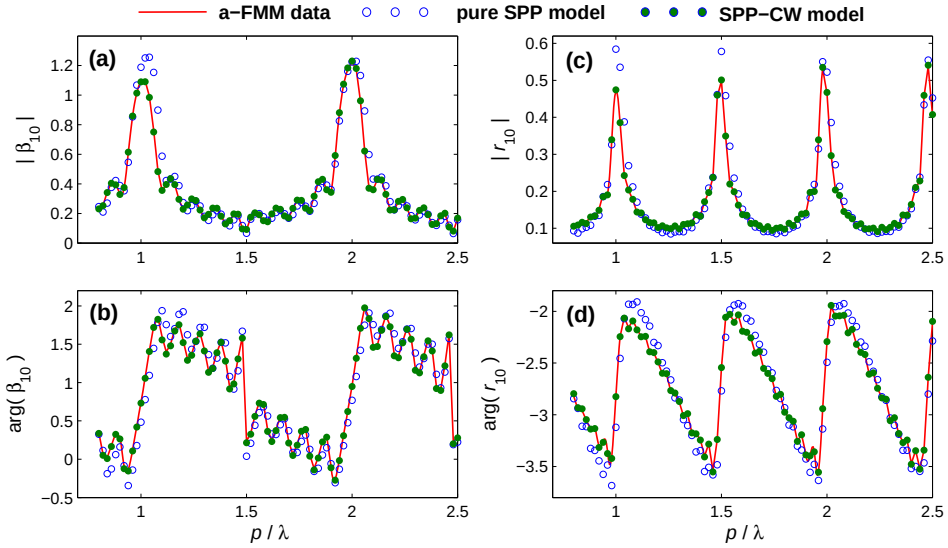

Figure 5. Comparisons among the a-FMM computational data (lines), the pure SPP model predictions (circles), and the SPP-CW model predictions (dots) on (a) $|\beta_{10}|$, (b) $\arg(\beta_{10})$, (c) $|r_{10}|$, and (d) $\arg(r_{10})$ as functions of the period p. The calculations are performed with $w = 0.4\lambda$, $h = 0.3\lambda$, $N = 10$.

Figure 5 compares the performances of the SPP-CW models and the pure SPP models. As clearly shown in the figure, the SPP-CW models predict the SPP excitation and reflection coefficients with high accuracy, in both amplitudes and phases, even when the periods are very small; whereas the accuracy of the pure SPP model predictions is improved as the periods increase. This is because for small periods, the generated CW field that is equal to (for the visible regime) or much larger than (for the infrared regime) the generated SPP field [22, 33] cannot be neglected; while for large periods, the generated SPP largely dominates because the generated CW has little influence on other grooves due to its fast damping characteristics. Furthermore, the optimized periods for the peak SPP excitation and reflection coefficients are well predicted by the pure SPP models and the SPP-CW models, indicating that the pure SPP models are accurate enough to predict the optimal periods, though there are some deviations in the peak values.

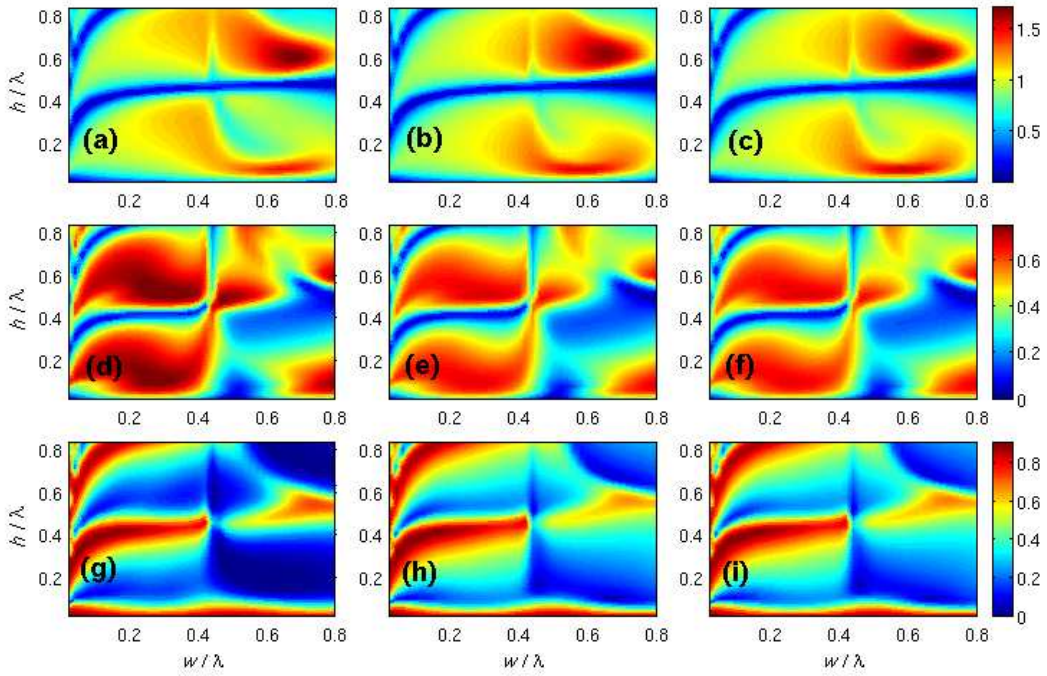

Figure 6. Comparisons among (a)(d)(g) the pure SPP model predictions, (b)(e)(h) the SPP-CW model predictions, and (c)(f)(i) the a-FMM computational data on (a)(b)(c) $|\beta_{10}|$, (d)(e)(f) $|r_{10}|$ and (g)(h)(i) $|t_{10}|$ as functions of the groove width w and height h. The calculations are performed with $p = \lambda$, $N = 10$.

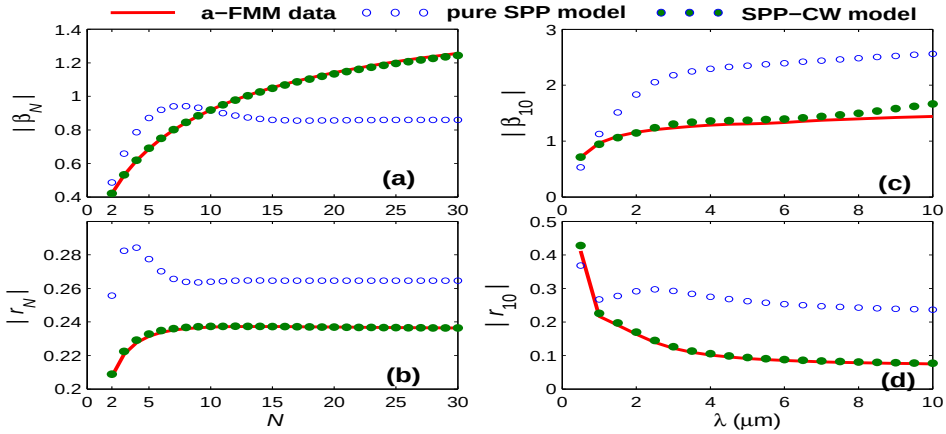

Figure 7. Comparisons among the a-FMM computational data (lines), the pure SPP model predictions (circles), and the SPP-CW model predictions (dots) on (a) $|\beta_N|$ and (b) $|r_N|$ with $\lambda = 800\,\text{nm}$ as functions of N; (c) $|\beta_{10}|$ and (d) $|r_{10}|$ with $N = 10$ as functions of the wavelength from the visible ($\lambda = 0.5\mu$m) to the thermal infrared regime ($\lambda = 10\mu$m). The calculations are performed with $w = 0.7\lambda$, $h = 0.3\lambda$, $p = \lambda$.

When the groove width and height are varying, the SPP-CW models and the pure SPP models are capable to capture all the salient features of the fully vectorial a-FMM computational data, as illustrated in figure 6. There are some deviations mainly in values for the pure SPP models, while the SPP-CW models predict with quantitative

accuracy on β_N, r_N and t_N, even when N is very large, as will be further discussed later. We should emphasize that their corresponding phase distributions are also accurately predicted by the SPP-CW models, which are not shown due to the space limitations. It is clear that the SPP-CW models are accurate even when the groove is very wide and very deep (w is up to 0.8λ and h is up to 0.85λ in figure 6). In other words, the SPP-CW models are applicable for the metallic grating composed of very wide and very deep subwavelength grooves.

There are pronounced deviations between the pure SPP model predictions and the a-FMM computational data for large period number N; whereas the SPP-CW models hold the accuracy for various N, as illustrated by figure 8(a)(b). As a result, with the SPP-CW models in forms of $4N$ linear equations, the SPP excitation and reflection coefficients by various N periodic grooves will be easily and accurately predicted starting from the information (i.e., the involved elementary coefficients) of a single groove.

The performance difference between the pure SPP models and the SPP-CW models is enlarged as the operating wavelength increases. The former is only accurate at visible and near-infrared frequencies, while the latter are accurate from the visible to the thermal infrared, as clearly illustrated in figure 8(c)(d). This is because at visible frequencies, the SPP contribution dominates, whereas the CW is preponderant in the long wavelength regime [22]. As a result, only the SPP-CW models are applicable over a broad spectral range.

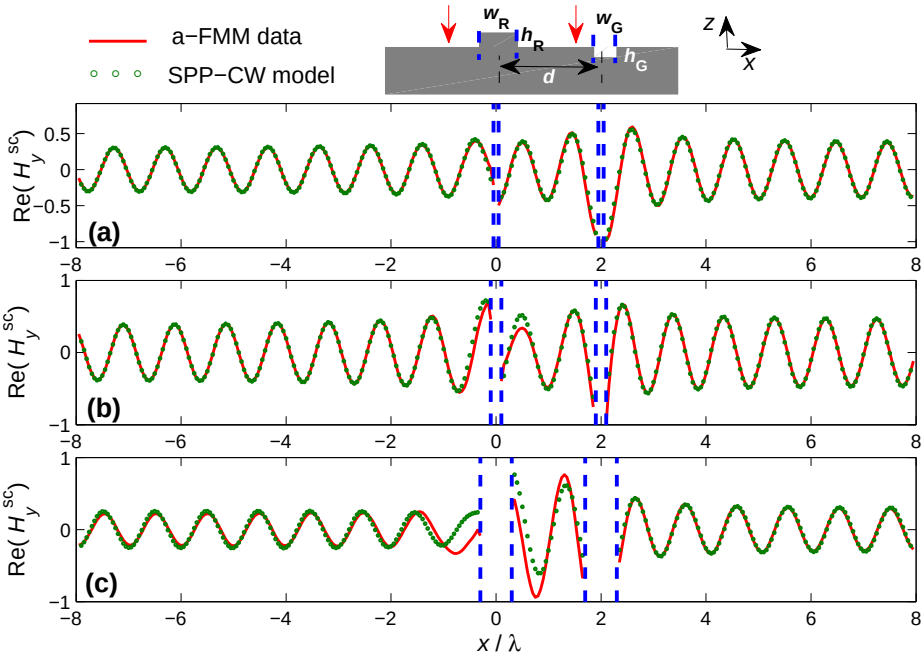

Figure 8. Comparisons among the a-FMM computational data (lines), and the SPP-CW model predictions (circles) on the scattered magnetic field at the surface for the structure composed of a metallic ridge (of width w_R and height h_R) and an air groove (of width w_G and height h_G). The calculations are performed with $w_R = h_R = w_G = w_G$, $= 0.1\lambda$ (a), $= 0.2\lambda$ (b), $= 0.6\lambda$ (c), $d = 2\lambda$.

4. Summary

We have theoretically investigated the interactions among the free-space light, the SPP mode and the CW in a subwavelength metallic grating composed of periodic or aperiodic surface defects. By adopting the concept of field decomposition, the scattering of CW was clarified and the CW-related coefficients were shown to be obtained though they were believed to be difficult or even impossible to define and calculate according to the classical scattering theory. We noticed that there is a remarkable relationship between the scattering coefficients of the SPP and those of the CW, which can be used to simplify the calculation. Based on the field decomposition and the elementary scattering processes of the light, the SPP and the CW by a single defect, the interactions in the excitation and the reflection of the SPP by N surface defects are embodied in two intuitive SPP-CW models. By comparing with the corresponding pure SPP models, the fully vectorial a-FMM computational data using exhaustive calculations with various parameters, including the periods, the groove widths and heights, the period numbers, and the operating wavelengths, the quantitative SPP-CW models were verified to be very accurate. We believe that the SPP-CW models are useful as they pave the way for the structure design and optimization with clear physical insight as well as a great reduce of the computational cost.

Acknowledgments

G. Li thanks Prof. P. Lalanne for fruitful discussions. This work was supported by the National Natural Science Foundation of China (NSFC) under grant 60772002, and by the State Key Laboratory of Advanced Optical Communication Systems and Networks, China.

References

[1] Devaux E, Ebbesen T W, Weeber J-C and Dereux A 2003 *Appl. Phys. Lett.* **83** 4936-8
[2] Ropers C, Neacsu C C, Elsaesser T, Albrecht M, Raschke M B and Lienau C 2007 *Nano Lett.* **7** 2784–8
[3] Evlyukhin A B, Reinhardt C, Evlyukhina E and Chichkov B N 2009 *Opt. Lett.* **34** 2237–9
[4] Ishi T, Fujikata J, Makita K, Baba T and Ohashi K 2005 *Jpn. J. Appl. Phys.* **44** L364
[5] Bhat R D, Panoiu N C, Brueck S R and Osgood R M 2008 *Opt. Express* **16** 4588–96
[6] Shackleford J A, Grote R, Currie M, Spanier J E and Nabet B 2009 *Appl. Phys. Lett.* **94** 083501
[7] López-Tejeira F *et al* 2007 *Nat. Phys.* **3** 324–8
[8] López-Tejeira F *et al* 2008 *New J. Phys.* **10** 033035
[9] Fu Z, Gan Q, Gao K, Pan Z and Bartoli F J 2008 *J. Lightwave Technol.* **26** 3699–703
[10] Nikitin A Y, García-Vidal F J and Martín-Moreno L 2009 *Appl. Phys. Lett.* **94** 063119
[11] Lu J, Petre C, Yablonovitch E and Conway J 2007 *J. Opt. Soc. Am.* B **24** 2268–72
[12] Lévêque G and Martin O J F 2006 *J. Appl. Phys.* **100** 124301
[13] Radko I P, Bozhevolnyi S I, Brucoli G, Martín-Moreno L, García-Vidal F J and Boltasseva A 2008 *Phys. Rev.* B **78** 115115
[14] Brucoli G and Martín-Moreno L 2010 *arXiv* 1009.4137v1
[15] Sánchez-Gil J A and Maradudin A A 2005 *Appl. Phys. Lett.* **86** 251106
[16] López-Tejeira F, García-Vidal F J and Martín-Moreno L 2005 *Phys. Rev.* B **72** 161405(R)
[17] López-Tejeira F, García-Vidal F J and Martín-Moreno L 2007 *Appl. Phys.* A **89** 251–8
[18] de León-Pérez F, Brucoli G, García-Vidal F J and Martín-Moreno L 2008 *New J. Phys.* **10** 105017
[19] Renger J, Grafström S, and Eng L M 2007 *Phys. Rev.* B **76** 045431
[20] Cao Q and Lalanne P 2002 *Phys. Rev. Lett.* **88** 057403
[21] Gay G, Alloschery O, de Lesegno B V, O'Dwyer C, Weiner J and Lezec H J 2006 *Nat. Phys.* **2** 262–7
[22] Lalanne P and Hugonin J P 2006 *Nat. Phys.* **2** 551–6
[23] Liu H and Lalanne P 2008 *Nature* **452** 728–31
[24] Cai L, Li G, Wang Z and Xu A 2010 *Opt. Lett.* **35** 127–9
[25] Cai L, Li G, Xiao F, Wang Z and Xu A 2010 *Opt. Express* **18** 19495–503
[26] Li G, Cai L, Xiao F, Pei Y and Xu A 2010 *Opt. Express* **18** 10487–99
[27] Aigouy L, Lalanne P, Hugonin J P, Julie G, Mathet V and Mortier M 2007 *Phys. Rev. Lett.* **98** 153902
[28] Yang X, Liu H and Lalanne P 2009 *Phys. Rev. Lett.* **102** 153903
[29] Li G, Cai L, Xiao F and Xu A 2010 *Opt. Lett.* **35** 3162–4
[30] Liu H and Lalanne P 2010 *Phys. Rev.* B **82** 115418
[31] Liu H and Lalanne P 2010 *J. Opt. Soc. Am.* A **27** 2542–50
[32] Vassallo C 1991 *Optical Waveguide Concepts* (Amsterdam: Elsevier)
[33] Lalanne P, Hugonin J P, Liu H and Wang B 2009 *Surf. Sci. Rep.* **64** 453–69
[34] Palik E D 1985 *Handbook of Optical Constants of Solids* (New York: Academic)
[35] Janssen O T A, Urbach H P and Hooft G W't 2006 *Opt. Express* **14** 11823–32
[36] Lalanne P, Hugonin J P and Rodier J C 2006 *J. Opt. Soc. Am.* A **23** 1608–15
[37] Silberstein E, Lalanne P, Hugonin J P and Cao Q 2001 *J. Opt. Soc. Am.* A **18** 2865–75